Patient-Specific Quantitation of Mitral Valve Strain by Computer Analysis of Three-Dimensional Echocardiography
A Pilot Study

Sagit Ben Zekry, MD; Jeff Freeman, MS; Aarti Jajoo, PhD; Jiwen He, PhD; Stephen H. Little, MD; Gerald M. Lawrie, MD; Robert Azencott, PhD; William A. Zoghbi, MD

Background—A paucity of data exists on mitral valve (MV) deformation during the cardiac cycle in man. Real-time 3-dimensional (3D) echocardiography now allows dynamic volumetric imaging of the MV, thus enabling computerized modeling of MV function directly in health and disease.

Methods and Results—MV imaging using 3D transesophageal echocardiography was performed in 10 normal subjects and 10 patients with moderate-to-severe or severe organic mitral regurgitation. Using proprietary 3D software, patient-specific models of the mitral annulus and leaflets were computed at mid- and end-systole. Strain analysis of leaflet deformation was derived from these models. In normals, mean strain intensity averaged 0.11±0.02 and was higher in the posterior leaflet than in the anterior leaflet (0.13±0.03 versus 0.10±0.02; $P<0.05$). Mean strain intensity was higher in patients with mitral regurgitation (0.15±0.03) than in normals (0.11±0.02; $P=0.05$). Higher mean strain intensity was noted for the posterior leaflet in both normal and organic valves. Regional valve analysis revealed that both anterior and posterior leaflets have the highest strain concentration in the commissural zone, and the boundary zone near the annulus and at the coaptation line, with reduced strain concentration in the central leaflet zone.

Conclusions—In normals, MV strain is higher in the posterior leaflet, with the highest strain at the commissures, annulus, and coaptation zones. Patients with organic mitral regurgitation have higher strain than normals. Three-dimensional echocardiography allows noninvasive and patient-specific quantitation of strain intensities because of MV deformations and has the potential to improve noninvasive characterization and follow-up of MV disease. **(*Circ Cardiovasc Imaging*. 2016;9:e003254. DOI: 10.1161/CIRCIMAGING.115.003254.)**

Key Words: echocardiography ■ follow-up studies ■ heart valve diseases ■ mitral regurgitation ■ mitral valve

The normally functioning mitral valve (MV) is complex; the saddle shape of the mitral annulus has been shown to influence leaflet deformation and to reduce stress on the valve leaflets.[1–6] The leaflets tissue properties and morphology are important as well. Myxomatous degeneration is the most common pathology in patients with mitral regurgitation (MR).[7] These organic MVs are characterized by alterations in collagen and cellular composition leading to thick and excess leaflet tissue, flattened and enlarged mitral annulus, and weak chordae. Consequently, leaflets may prolapse or flail, resulting in significant MR. MV deformation during the cardiac cycle can be variable within various regions of the normal MV and in valve disease states. The majority of previous studies evaluating MV strain were based on animal models, whereby crystals attached to the mitral apparatus and imaged with 3-dimensional (3D) cameras provided strain measurements.[1,2,8–13] With recent technical advances in 3D echocardiography, dynamic volumetric imaging and tracking of the MV apparatus can now be performed in real time and enable direct computerized study of MV motion and deformation in humans, without the need for invasive instrumentation. The aim of the present study was, first, to quantitate patient-specific global and regional dynamic deformations of the MV apparatus in a normal patient population and, second, to evaluate whether patients with organic MR have significant alterations in the intensity of global strain and its regional distribution.

See Editorial by Watanabe
See Clinical Perspective

Methods

Patient Population

The patient population was prospectively enrolled and included individuals with a normal heart by echocardiography who underwent a transesophageal echocardiogram for clinical reasons such

Received February 4, 2015; accepted November 15, 2015.

From the Echocardiography Department (S.B.Z., S.H.L., W.A.Z.) and Department of Cardiovascular and Thoracic Surgery (G.M.L.), Houston Methodist DeBakey Heart and Vascular Center, TX; Department of Cardiology, Non Invasive Cardiology Unit, Affiliated with the Leviev Heart Center, Sheba Medical Center and Sackler School of Medicine, Tel Aviv University, Tel Aviv, Israel (S.B.Z.); and Department of Mathematics, University of Houston, TX (J.F., A.J., J.H., R.A.).

The Data Supplement is available at http://circimaging.ahajournals.org/lookup/suppl/doi:10.1161/CIRCIMAGING.115.003254/-/DC1.

Correspondence to William A. Zoghbi, MD, Houston Methodist DeBakey Heart and Vascular Center, 6550 Fannin St, SM 677, Houston, TX 77030. E-mail wzoghbi@houstonmethodist.org

as potential sources of emboli or fever, and patients with organic moderate-to-severe or severe MR undergoing transesophageal echocardiography before MV repair. MR severity was graded using the integrative and quantitative approach of the American Society of Echocardiography.[14] Patients with arrhythmias or poor images were excluded. The study was approved by the human research review board of Houston Methodist Hospital. All patients provided written informed consent.

Three-Dimensional Echocardiography Protocol

Three-dimensional transesophageal echocardiographic imaging was performed using an IE-33 ultrasound system (Philips, Andover, MA) with X7-2t probe. The imaging protocol included a midesophageal, full volume acquisition, concentrating on the MV apparatus and aiming at visualizing the mitral annulus throughout the cardiac cycle, adjusting settings to maximize frame rate. The 3D images were digitally stored and analyzed at a later time.

Patient-Specific MV Modeling

Patient-specific MV modeling was described in more details in our 2 previous technical articles.[15,16] To summarize, using Slicer 3D software, the mitral annulus and leaflets were tagged on the 3D echo images at both mid- and end-systole by an expert echocardiographer (S.B.Z.). End-systole was defined as the last frame when the aortic valve was open, and end-diastole as the last frame when the MV was open. Several variants of Bi-Cubic Splines (B-splines) fitting were then applied (using MATLAB procedures[15]) to compute patient-specific static models of mitral leaflets, annulus, and coaptation line (Figure 1). All static mitral leaflets models were then discretized into point meshes of 1500 to 3000 points (≈0.5-mm mesh size). Similarly, all our patient-specific mitral annulus models were discretized into meshes of 300 to 500 points.

MV Dynamic Tracking

Automated registration of 3D echocardiographic image sequences is crucial to quantify cardiac deformations[15,17] and to compute mitral leaflets strain. MV apparatus deformations were modeled by diffeomorphisms of R^3,[18–21] which are arbitrary invertible and continuously differentiable 3D spatial deformations. This diffeomorphic registration technique, as detailed in our previous articles,[15,16] is similar to the powerful computational anatomy methods introduced to register 3D images of brains,[18,22] and analogous diffeomorphic approaches have been successfully used to reconstruct 3D deformations of heart muscle or heart chambers.[23–25] The key registration principle is the computerized minimization of a Cost Function, controlling deformation velocities at several thousand points of the MV leaflets. This cost function simultaneously penalizes undesirable deformations features such as high kinetic energies and strong geometric registration errors, as well as high disparities of image voxels intensities along deformation trajectories. Cost minimizing MV deformations are then automatically forced to smoothly match all the intermediary MV snapshots captured in 3D by the successive echocardiographic frames. This computerized approach successfully reconstructed and tracked patient-specific detailed MV deformations for all patients studied. A dynamic example of MV deformation tracking is shown in the clip; see also an example of deformation tracking for an anterior leaflet (AL) in Figure 2 and Supplemental Digital Content.

Strain Computation

For each patient, the strain tensors at several thousands of MV leaflets points were then derived from the computer-reconstructed patient-specific MV deformations between mid- and end-systole. Our mathematical computation of the strain tensor does not require any assumption on tissue elasticity. Each MV apparatus deformation model generates the dynamic trajectories of several thousands of leaflets points *x* between the times of midsystole and end-systole. For each initial leaflet point x, and any small tissue patch P(x) around x, the computed deformation of P(x) between midsystole and end-systole approximately multiplies small lengths by a computable dimensionless factor g(x)>0, called the geometric strain at x.[15] Tissue deformations around x are dilating if g(x)>1, and contracting if g(x)<1. The leaflet strain intensity SI(x) at x is then defined as the magnitude of length dilation (or contraction) around x, given by $\mathrm{SI}(x) = |g(x) - 1|$. Strain intensity SI(x) is computed at several thousand points x of each leaflet to characterize the distribution of SI values on the leaflet surface. These strain maps were then displayed on each patient-specific model. Mean strain values for normal and organic MV as well as mean strain for anterior and posterior leaflets (PL) were computed. Figure 3 displays examples of strain maps for 1 normal and 1 organic valve.

Leaflet Geometric Zones

To study the patient-specific localization of higher strain areas on both the anterior and the PLs, we defined 8 geometric regions of interest for each leaflet, based on the computer-reconstructed patient's leaflet shape at midsystole. Figure 4 displays these 8 geometric zones for the PL of 1 patient. The 3 scallops Sc1, Sc2, and Sc3 were identified at both midsystole and end-systole by 2 cardiology experts, tagging points along the annulus and the coaptation line (S.B.Z. and S.L.) to pin down the 2 boundaries separating the 3 scallops. A computer treatment based on this tagging then generated the scallops Sc1, Sc2, and Sc3 with areas, respectively, equal to 25%, 50%, and 25%, with error margins of 2%.

The remaining 5 zones were constructed as follows. The leaflet zone adjacent to the annulus Z_{ann} and the coaptation zone Z_{coapt} were defined as all leaflet points within a short distance of the annulus or coaptation line so that the areas of Z_{ann} and Z_{coapt} were both equal to 20% of total leaflet area (Figure 4). The boundary zone of the leaflet, Z_{bound} was defined as the sum of Z_{ann} and Z_{coapt}. The center zone Z_{center} is the leaflet area excluding the boundary zone. Finally, a commissure

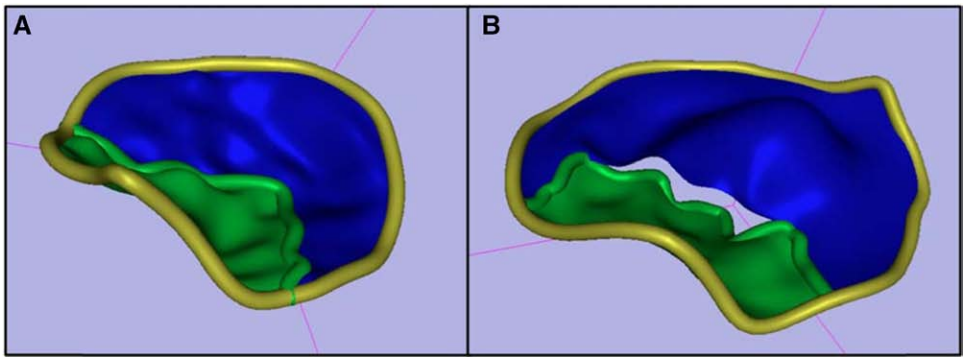

Figure 1. Two patient-specific static mitral valve models: normal patient (**A**) and organic mitral regurgitation patient (**B**), both at midsystole. Color scheme: Mitral annulus in gold, anterior leaflet in green, and posterior leaflet in blue.

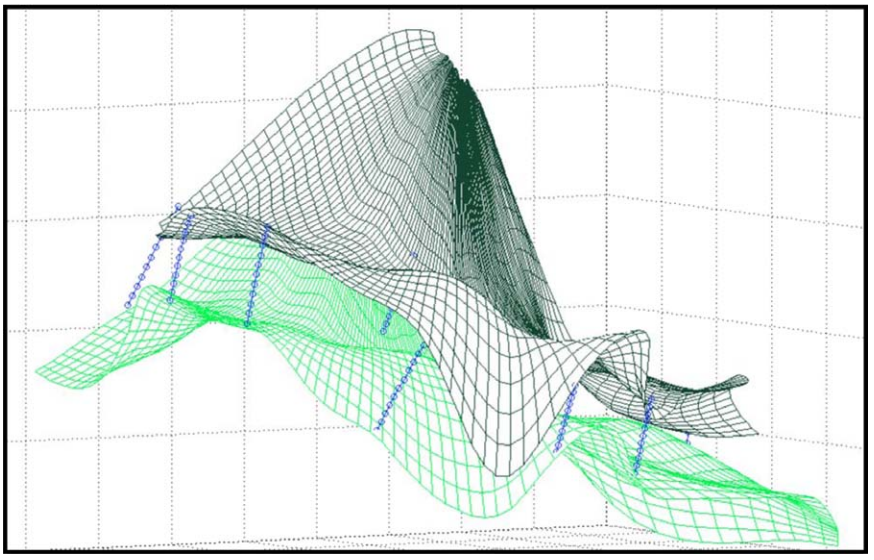

Figure 2. Patient-specific algorithmic tracking of anterior leaflet dynamic deformations for a regurgitation case. Only a few of the several thousand reconstructed deformation trajectories are shown (in blue) to facilitate visualization.

zone, Z_{comm}, was the area of leaflets at the 2 commissures extending to the annulus and was set at 8% of total leaflet area (Figure 4). All these geometric zones were computed at midsystole only because the corresponding regional mean strain intensities were also computed and displayed only at midsystole.

High Strain Concentration

To highlight the localization and extent of high strain (HS) in various zones, a HS concentration HSC(Z) was computed for each one of the leaflet geometric zones. The HS points of the mitral leaflet were defined as all leaflet points, where SI was larger than the patient-specific 75th percentile of strain intensities. Within any leaflet, the HS area is then always equal to 25% of total leaflet area. For each leaflet zone Z, we computed its HSC HSC(Z) as the ratio of the area of HS within Z to the total area of Z, so that HSC(Z)=area (HS∩Z)/area (Z), and is always <1. For randomly selected large zones, HSC(Z) is typically close to 0.25, so that values of HSC(Z) >0.35 indicate strong concentrations of HS points within the zone Z.

Reproducibility

Reproducibility of global and regional strain and HSC was performed after randomly perturbing the tagging points on the MV in normal and organic MR valves and applying the computer algorithm for quantitation of strain globally and regionally as described above. Absolute difference, mean, and percent change in strain and HSC were computed.

Statistical Analysis

Patient group averages for patients' demographic data, MV geometric variables, MV leaflets strain intensities, regional strain concentrations are expressed as mean±SE. Differences in means (normal versus organic, midsystole versus end-systole, and anterior versus posterior) were tested as follows and considered significant for $P<0.05$. Within the same group of 10 patients, comparing the mean values of any MV geometric variable or strain requires the elimination of patient effects. This was achieved by implementing linear models with mixed random effects and computing the associated P value. This was applied to comparisons within same group of variables at midsystole versus end-systole, anterior versus PLs, and mean HS concentrations HSC between different leaflet zones. To compare mean values of variables between the distinct groups of organic MR and normals, patient effects become irrelevant and hence standard t test was used in these instances.

For each leaflet and each patient, strain intensities were computed at several thousand leaflet points, and the distribution of these strain intensities was then characterized by its percentiles Q (5%), Q (10%), …, Q(95%), which were also displayed graphically as percentile curves. To compare strain distributions across patients, we have

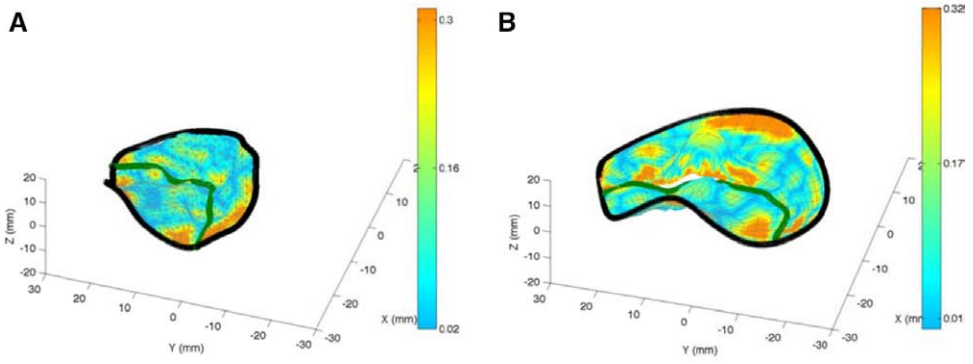

Figure 3. Patient-specific mitral leaflets strain intensities displayed at midsystole for a typical normal mitral valve (**A**) and for a typical organic valve with mitral regurgitation valve (**B**). The strain intensities color code range from dark orange for high strain to dark blue for low strain.

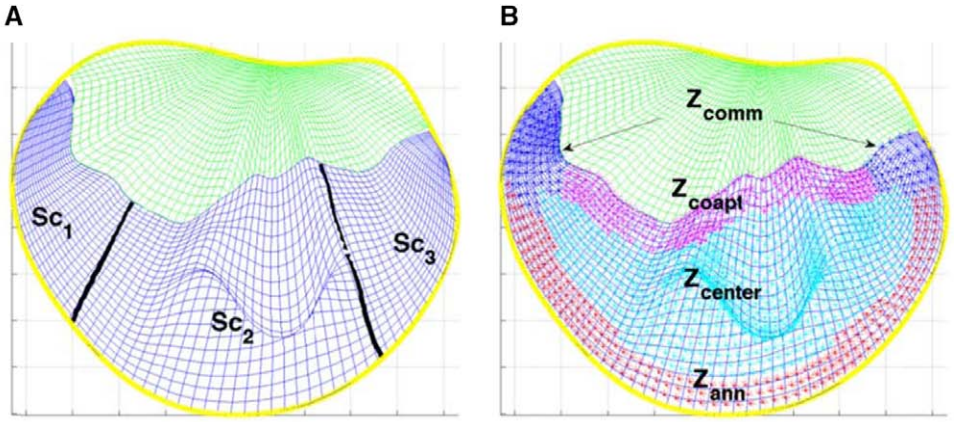

Figure 4. Patient-specific computed leaflet zones for one typical posterior leaflet. Anterior leaflet zones are omitted for visual clarity. **A**, The 3 posterior leaflet scallops (Sc1, Sc2, and Sc3), whereas **B** displays the 5 other geometric zones: commissures (Z_{comm}), coaptation (Z_{coapt}), annulus (Z_{ann}), and center (Z_{center}). The boundary zone Z_{bound} is the union of the annulus and coaptation zones.

systematically compared the corresponding percentiles curves. Given 2 large data sets {X1, X2, . . . XN} and {Y1, Y2, . . . YM}, with N, M>1000, one classically says[21] that the X values are stochastically smaller than the Y values if each percentile $Q_X(z\%)$ of the X values, for every percentage 0%<z%<100%, is inferior or equal to the corresponding percentile Q_Y (z%) of the Y values. This can be verified visually by plotting the 2 percentile curves Q_X and Q_Y to check whether the curve Q_X indeed lies below the curve Q_Y. The reliability of the statement X is stochastically smaller than Y is evaluated by its *P* value, computed by a Kolmogorov–Smirnov test (K–S test) and is considered significant if its $P<0.05$.

Results

The study population included 10 patients with a normal heart and MV and 10 patients with moderate-to-severe or severe organic MR (Table 1). Patients with MR had larger left ventricular volumes, similar ejection fraction, and lower systolic blood pressure than the normal group. Among the 10 patients with organic MR, there were 5 cases of flail P2, 1 case of (flail P2+P1 prolapse), 1 case of (flail P2+P3 prolapse), and 1 case of (flail P2+A2 prolapse).

MV Geometry

Patients with organic MR had enlarged mitral annulus, annulus circumference, and anterior-posterior diameter, whereas the annulus height was reduced (Table 2). Both groups showed annulus dynamicity from mid- to end-systole where the annulus was more flattened and enlarged at end-systole (Table 2). AL area was comparable in the 2 groups. As expected, the PL was larger in the organic group where the ratio of leaflet area (posterior versus anterior) was significantly higher than for normals at both mid- and end-systole (Table 2).

Mitral Leaflet Strain

Global Strain

Mean strain intensities for the whole MV as well as its AL and PL in normal and patients with organic MR are shown in Figure 5. All results in this paragraph were statistically significant ($P<0.05$). Group average of mean SI was higher in PL than in AL, for normals (0.13±0.01 versus 0.10±0.01) and for organic MR (0.19±0.016 versus 0.13±0.01). Group averages of mean SI were higher in organic MR leaflets than in normals, for whole valves (0.15±0.01 versus 0.11±0.01), for PL (0.19±0.016 versus 0.13±0.01), and for AL (0.13±0.01 versus 0.10±0.01). Group averages of strain values distributions for AL and PL leaflets were stochastically higher for organic MR than for normals (Figure 6; K–S test, $P<0.05$).

Regional Strain

The regional analysis of HSC in the 8 zones of MV leaflets is summarized in Table 3. Each MV leaflet (normals and organic MR) showed HSC to be highest for the commissural zone and lowest for the center zone. In general, HSC(Z_{bound}) for the boundary zone comprising narrow bands along the annulus and coaptation lines had intermediate values, higher than HSC (Z_{center}) and lower than HSC (Z_{comm}). For 19 of the 20 patients, elevated HSC were seen in the commissures as well as along the annulus and coaptation line, whereas the leaflet center had low HSC (Figure 7).

For each one of the 8 zones, the group averages of HSC(Z) did not significantly differ between normals and organic MR patients. For the 3 valve scallops, in both groups of patients, the highest strain concentration was seen in Sc1 and were elevated in both AL and PL. Lower values were seen in Sc2 and Sc3 (Table 3).

Reproducibility

Global strain ranged between 0.12 and 0.23 in the retested patients. The difference in global MV strain after retesting ranged between 0.002 and 0.022, mean of 0.04. Mean percent change in global strain was 5% (range, 5%–10%). Regional strain analysis yielded a mean percent change of 8% (range, 0.0%–13.5%). For HSC variability, mean % difference was 4% (range, 2%–6%).

Discussion

Three-dimensional transesophageal echocardiography allowed a study of MV deformation in healthy and organic valves. Patient-specific MV models were computer generated, and strain distributions were derived algorithmically, allowing comparative analysis of global and regional strain. Patients

Table 1. Mean Patients Data for the Normal and the Organic MR Group

Variable	Normal Group	Organic MR Group
No. of patients	10	10
Age, y	55±1.9	64±4.1
No. of male patients	6	9
BSA, m^2	1.93±0.1	2.1±0.13
Systolic blood pressure, mm Hg	136±8.5	109±6.3
Diastolic blood pressure, mm Hg	74±6	61±4.1
Heart rate, bpm	70±4.1	69±3.5
Left ventricular ejection fraction, %	65±1.6	65±2.8
No. of imaging frames/cardiac cycle	24±2	23±2
Left ventricle end-diastolic volume, mL	124±9.2	196±12*
Left ventricle end-systolic volume, mL	48±4.1	74±1*
Regurgitation volume, mL	N/A	63.8±9.5
Effective regurgitation orifice area, cm^2	N/A	0.4±0.1

BSA indicates body surface area; and MR, mitral regurgitation.
*Mean value for organic MR group is larger than for Normal group with $P<0.05$

with organic MR had higher strain than normal subjects; for both groups, strain intensities were higher in the PL than in the AL. Overall, HSC was highest in the commissural zone, intermediate in the annulus and coaptation zones, and lowest in the central zone.

MV Modeling

The majority of previous studies evaluating MV deformation and leaflet tissue stress parameters have used surgically implanted crystals in animal models[1–3,6,8,10,13] and camera recordings of crystals motion. Other studies have combined similar in vivo data with parameterized elasticity models implemented by customized finite elements software.[26–28] These studies have generally focused on stress analysis via elasticity models of various complexities. Limited information on SI distribution on the whole MV leaflets remains, particularly in man. A combination of 3D models with 3D echocardiography was used to investigate the effect of annular saddle shape on leaflet curvature in 3 patients,[6] and in animal models.[4,6,29] Human MV models based on 10 normals were used to emulate mitral leaflets deformation during isovolumic contraction.[30] An MV model based on 3D echo images for 2 normals and 2 patients with MR[11,12] aimed to model valve leaflet strain assuming that papillary muscles remain at constant distance from the mitral leaflets.[31,32]. Ge et al[28] used magnetic resonance imaging and 3D echo coregistered images to create finite element model to predict stress changes in a single patient after valve repair. Because the in vivo biomechanical properties of human MV leaflets are not yet well quantified, all the above-mentioned investigations had to use elasticity model parameters derived from animal data.[4,29]

The present study deliberately avoided to compute MV stress and focused instead on quantitating and comparing the distributions of strain intensities in normal and diseased valves. Patient-specific MV models allowed implementation of a computer intensive reconstruction of MV deformations during systole, where visual tagging of mitral leaflet tips is more accurate. This proved especially challenging for organic valves with prolapsed and flail segments where complex tissue folding was noted. Patient-specific leaflet deformations were reconstructed by computerized diffeomorphic registration of the 3D echocardiography images. We computed the planar strain tensor at several thousand points on the MV, generated by leaflet deformation.[33] Our comparative strain studies across patients focuses then on the patient-specific distributions of strain intensities on each MV leaflet. This approach, built around leaflets strain intensities as indicators of MV tissue fatigue, has several advantages. First, it can be easily and noninvasively implemented for human subjects through computer analysis of standard 3D echocardiography. Second, we did not need to introduce any elasticity hypotheses for MV leaflets tissue for strain calculation. Indeed, realistic MV elasticity models are anisotropic and highly nonlinear so that in most publications, parametrization of

Table 2. Comparison of MV Geometric Variables

	Normal Group		Organic MR Group	
Geometric Variables	Midsystole	End-Systole	Midsystole	End-Systole
MV annulus				
Area in projection, cm^2	10.4±0.7	11.8±0.8*	15.2±0.8†	16.5±0.1*†
Circumference, mm	129±4.6	132.2±4.6*	151.9±3.6†	155±4.1*†
Height, mm	13.6±0.5	11.7±0.7‡	13.0±0.5	12.3±0.5‡
Anterior-posterior diameter, mm	36.7±1.3	39.7±1.1*	42.5±1.2†	45.4±1.2*†
MV leaflets				
AL area, mm^2	647±28	667±85*	613±65	644±63*
PL area, mm^2	643±52	710±183*	899±66†	932±71†
Ratio (PL area/AL area)	0.98±0.06	1.05±0.06*	1.5±0.1†	1.5±0.1†

AL indicates anterior leaflet; MR, mitral regurgitation; MV, mitral valve; and PL, posterior leaflet.
*Mean value at end-systole>mean value at midsystole, $P<0.05$.
†Mean value for organic MR>mean value for normal, $P<0.05$.
‡Mean value at end-systole<mean value at midsystole, $P<0.05$.

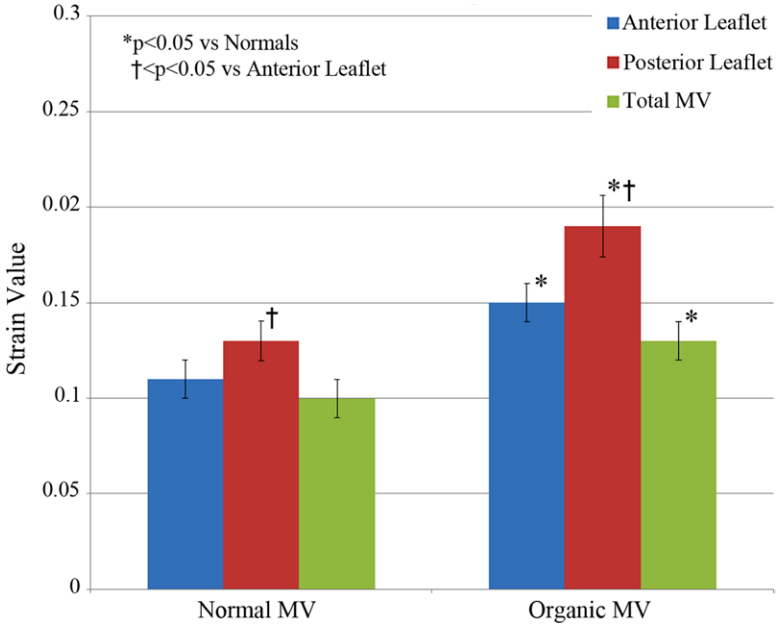

Figure 5. Mean strain values for the whole mitral valve (MV) as well as for the anterior and posterior leaflets in normals when compared with patients with organic mitral regurgitation. Mean and SE bars are shown.

elasticity models for human MVs relies on stress measurements made in vivo on animal models. Our approach was hence much easier to compute than the analogous stress values. Moreover, the comparison of strain intensities across different patients is robust to reconstruction errors. Because these comparisons rely on percentile curves computed from ≈3000 strain values for each leaflet, the error on any strain percentile is 25 to 50 times smaller than the errors affecting individual strain values.

Strain in Normal MV and Organic MV Regurgitation

Global MV Strain

In normal MV, strain in the PL was higher than in the AL and was maintained in organic MV. This finding may be because of the lesser tensile strength at pathology[34] and is of interest clinically as most mitral annular calcifications occur in the posterior mitral annulus,[35] invoking higher strain in this region as a possible contributing mechanism for posterior annular calcifications in the aging MV. In general, strain for organic valves was higher than for normal valves, globally and in each valve leaflet. This was seen despite a lower systolic blood pressure in the group of organic valves, implying that this difference in strain is likely to be higher if blood pressure was similar.

The organic MVs had, as expected, a larger annulus and PL size than normals. The higher systolic deformation in organic MV could be explained, in part, by these geometric differences and, in addition, by alterations to the saddle shape of the annulus.[1–3] Finally, the different cellular and structural composition of organic valves cannot be ignored. In myxomatous valves, the normally collagen-rich valvular fibrosa becomes infiltrated by proteoglycans and an abundance of

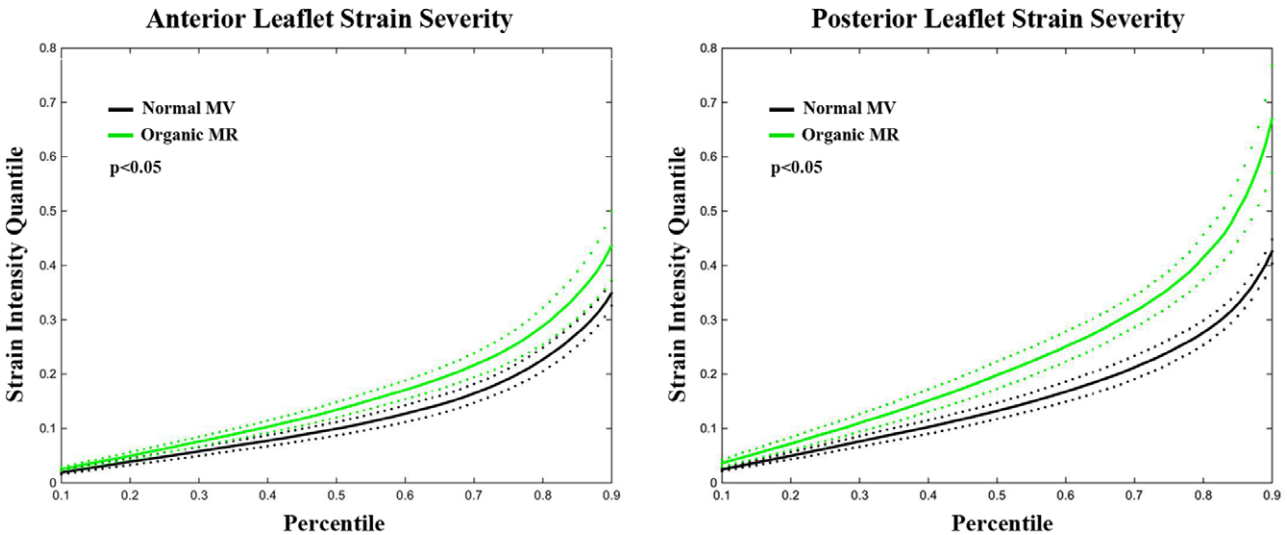

Figure 6. Mean strain percentile curves and respective 95% confidence limits in anterior and posterior leaflets of normal mitral valves (MVs) and organic mitral regurgitation. Strain values are higher in organic mitral regurgitation (MR) than in normal valves.[18]

Table 3. Comparison of Mean Regional HSC for 8 Zones of the Mitral Valve Leaflets

	Normal Group (n=10)		Organic MR Group (n=10)	
Leaflet Zones	Anterior Leaflet	Posterior Leaflet	Anterior Leaflet	Posterior Leaflet
Z_{comm}	0.44±0.06*	0.37±0.07	0.44±0.05*	0.37±0.05
Z_{ann}	0.36±0.02	0.31±0.03	0.31±0.05	0.35±0.06
Z_{coap}	0.35±0.03	0.32±0.02	0.36±0.03	0.37±0.04
Z_{bound}	0.35±0.01	0.31±0.02	0.32±0.03	0.35±0.03
Z_{center}	0.19±0.01†	0.21±0.01†	0.21±0.02†	0.19±0.02†
Sc1	0.42±0.04‡§	0.35±0.04‡§	0.34±0.04§	0.32±0.03§
Sc2	0.14±0.02	0.23±0.02	0.16±0.02	0.24±0.02
Sc3	0.29±0.02‖	0.18±0.03	0.33±0.04‖	0.20±0.02¶

HSC indicates high strain concentration; Z_{ann}, annular boundary zone; Z_{bound}, whole boundary zone; Z_{center}, central zone; Z_{coap}, coaptation boundary zone; and Sc1, Sc2, and Sc3, mitral valve scallops.
*HSC(Z_{comm})>HSC(Z_{bound}) (P<0.05).
†HSC(Z_{center})<HSC(Z_{bound}), HSC(Z_{comm}), HSC(Z_{ann}), and HSC(Z_{coap}) (each, P<0.05).
‡HSC(Sc1)>HSC(Sc3) (P<0.05).
§HSC(Sc1)>HSC(Sc2) (P<0.05).
‖HSC(Sc3)>HSC(Sc2) (P<0.05).
¶HSC(Sc3)<HSC(Sc1) (P<0.05).

matrix-degrading enzymes, leading to thickening and weakening of valve tissue.[36–38] Transforming growth factor-β, decorin, and fibrillin have also been implicated in pathological extracellular matrix remodeling leading to myxomatous valve disease, which undoubtedly contribute to alterations in valve deformation properties.[38,39]

Regional Strain

Regional analysis of HSC revealed variable patterns: the highest mean HSC was noted in the area of the commissures and in Sc1, followed by the boundary zone, whereas the lowest values were seen in the center zone (Table 3; Figure 7). In general, any leaflet edge presented higher deformation, and hence higher strain values, consistent with observations in sheep.[9] The strain in the coaptation zone is likely influenced by annular dynamics, the pressure gradient across the valve, as well as papillary muscle function and chordal stress. In organic MVs, alterations in tissue properties and valve/annular size are likely contributors to the changes in strain, which are consistent with previous simulation studies.[10,13]

A reduced HSC was noted in the Sc2 of the AL for both patient groups. This may be explained, in part, by the fact that the Sc2 of the AL is attached to the aortic-mitral continuity and is characterized by fibrotic tissue, which probably is more resistant to deformation. The higher HSC in the posterior Sc2 seen in both normal valves and in organic MR raise the possibility of contribution of strain to the pathophysiology of prolapse and flail PLs—clinical entities that are more prevalent in this MV region.

Limitations

The population involved small patients groups, limited by the complexity of the patient-specific dynamic MV modeling and the intricacy of the strain computation. To our knowledge, this is the largest human MV dynamic modeling study. Milder MR in organic MV was not evaluated but is planned. We studied only systolic deformation and chose midsystole, where highest deformation and pressure occurs, and end-systole where deformation is much less. The 3D echocardiograms are gated studies; however, we chose only high-quality images with minimal stitch artifacts.

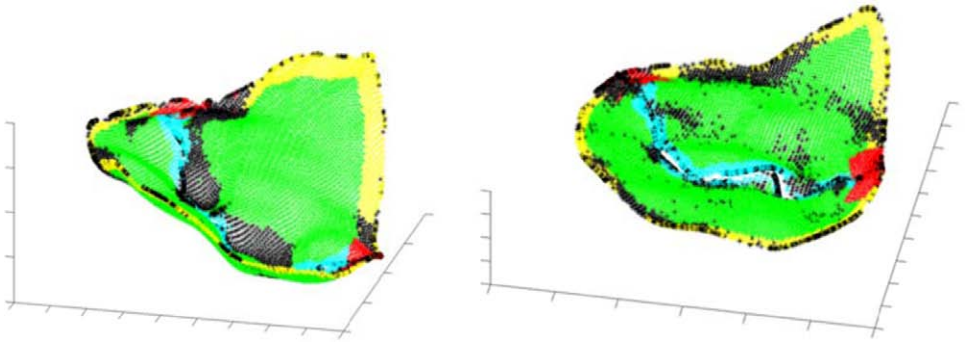

Figure 7. Example of high strain concentration (HSC) for normal valve (**left**) and organic valve (**right**). The points with strain intensities higher than the 75th percentile of strain values are shown in black. Z_{comm} is red, Z_{coapt} is blue, Z_{ann} is yellow, and Z_{center} is green. Note the presence of HSC around the annulus, in the commissure and coaptation zones.

Conclusion and Clinical Implications

Computerized analysis of 3D echocardiography allowed in vivo, patient-specific quantification of MV strain intensities in normals and patients with organic MR. Patients with organic MV had increased strain intensities when compared with normals, globally as well as in the AL and PL. Higher strain concentrations were systematically noted near the commissures and leaflets boundary zones, whereas lower strain values were observed in the center zone. Our approach could provide new evaluation tools for quantification of global and regional SI distributions in vivo, which may have important implications in further understanding MV disease pathophysiology and progression, and in comparative investigations of surgical techniques involved in MV repair that aim at restoring MV geometry and stress and strain reduction for possible improved durability.

Sources of Funding

Dr Azencott and University of Houston collaborators were supported by grant NSF-0811133 from 2008 to 2011; Dr Zekry was partly funded by a grant from 2009 to 2011 and by the John and Maryanne McCormack Cardiology Fund, Houston, TX.

Disclosures

None.

References

1. Jimenez JH, Liou SW, Padala M, He Z, Sacks M, Gorman RC, Gorman JH III, Yoganathan AP. A saddle-shaped annulus reduces systolic strain on the central region of the mitral valve anterior leaflet. *J Thorac Cardiovasc Surg*. 2007;134:1562–1568. doi: 10.1016/j.jtcvs.2007.08.037.
2. Amini R, Eckert CE, Koomalsingh K, McGarvey J, Minakawa M, Gorman JH, Gorman RC, Sacks MS. On the *in vivo* deformation of the mitral valve anterior leaflet: effects of annular geometry and referential configuration. *Ann Biomed Eng*. 2012;40:1455–1467. doi: 10.1007/s10439-012-0524-5.
3. Padala M, Hutchison RA, Croft LR, Jimenez JH, Gorman RC, Gorman JH III, Sacks MS, Yoganathan AP. Saddle shape of the mitral annulus reduces systolic strains on the P2 segment of the posterior mitral leaflet. *Ann Thorac Surg*. 2009;88:1499–1504. doi: 10.1016/j.athoracsur.2009.06.042.
4. Ryan LP, Jackson BM, Hamamoto H, Eperjesi TJ, Plappert TJ, St John-Sutton M, Gorman RC, Gorman JH III. The influence of annuloplasty ring geometry on mitral leaflet curvature. *Ann Thorac Surg*. 2008;86:749–760; discussion 749. doi: 10.1016/j.athoracsur.2008.03.079.
5. Kunzelman KS, Reimink MS, Cochran RP. Annular dilatation increases stress in the mitral valve and delays coaptation: a finite element computer model. *Cardiovasc Surg*. 1997;5:427–434.
6. Salgo IS, Gorman JH III, Gorman RC, Jackson BM, Bowen FW, Plappert T, St John Sutton MG, Edmunds LH Jr. Effect of annular shape on leaflet curvature in reducing mitral leaflet stress. *Circulation*. 2002;106:711–717.
7. Nkomo VT, Gardin JM, Skelton TN, Gottdiener JS, Scott CG, Enriquez-Sarano M. Burden of valvular heart diseases: a population-based study. *Lancet*. 2006;368:1005–1011. doi: 10.1016/S0140-6736(06)69208-8.
8. Rausch MK, Bothe W, Kvitting JP, Göktepe S, Miller DC, Kuhl E. *In vivo* dynamic strains of the ovine anterior mitral valve leaflet. *J Biomech*. 2011;44:1149–1157. doi: 10.1016/j.jbiomech.2011.01.020.
9. Stevanella M, Krishnamurthy G, Votta E, Swanson JC, Redaelli A, Ingels NB Jr. Mitral leaflet modeling: Importance of *in vivo* shape and material properties. *J Biomech*. 2011;44:2229–2235. doi: 10.1016/j.jbiomech.2011.06.005.
10. Sacks MS, He Z, Baijens L, Wanant S, Shah P, Sugimoto H, Yoganathan AP. Surface strains in the anterior leaflet of the functioning mitral valve. *Ann Biomed Eng*. 2002;30:1281–1290.
11. Rim Y, McPherson DD, Chandran KB, Kim H. The effect of patient-specific annular motion on dynamic simulation of mitral valve function. *J Biomech*. 2013;46:1104–1112. doi: 10.1016/j.jbiomech.2013.01.014.
12. Rim Y, Laing ST, Kee P, McPherson DD, Kim H. Evaluation of mitral valve dynamics. *JACC Cardiovasc Imaging*. 2013;6:263–268. doi: 10.1016/j.jcmg.2012.10.017.
13. He Z, Ritchie J, Grashow JS, Sacks MS, Yoganathan AP. *In vitro* dynamic strain behavior of the mitral valve posterior leaflet. *J Biomech Eng*. 2005;127:504–511.
14. Zoghbi WA, Enriquez-Sarano M, Foster E, Grayburn PA, Kraft CD, Levine RA, Nihoyannopoulos P, Otto CM, Quinones MA, Rakowski H, Stewart WJ, Waggoner A, Weissman NJ; American Society of Echocardiography. Recommendations for evaluation of the severity of native valvular regurgitation with two-dimensional and Doppler echocardiography. *J Am Soc Echocardiogr*. 2003;16:777–802. doi: 10.1016/S0894-7317(03)00335-3.
15. Ben Zekry S, Lawrie GM, Little SH, Zoghbi WA, Freeman J, Jajoo A, Jain S, He J, Martynenko A, Azencott R. Comparative evaluation of mitral valve strain by deformation tracking in 3D-Echocardiography. *J Cardiovs Tech*. 2012; 3:402–412.
16. Azencott R, Glowinski R, He J,Hoppe R, Jajoo A, Li Y, Martynenko A, Hoppe R, Ben Zekry S, Little SH, Zoghbi WA. Diffeomorphic matching and dynamic deformable surfaces in 3D medical imaging, *Comput Meth Appl Math* 2010;10:235–274.
17. Heyde B, Cygan S, Choi HF, Lesniak-Plewinska B, Barbosa D, Elen A, Claus P, Loeckx D, Kaluzynski K, D'hooge J. Regional cardiac motion and strain estimation in three-dimensional echocardiography: a validation study in thick-walled univentricular phantoms. *IEEE Trans Ultrason Ferroelectr Freq Control*. 2012;59:668–682. doi: 10.1109/TUFFC.2012.2245.
18. Beg MF, Miller MI, Trouve A, Younes L. Computing large deformation metric mappings via geodesic flows of diffeomorphisms, *Int. J. Comp. Vis.,* 2005; 61:139–157.
19. Guo H, Rangarajan A, Joshi S, Younes L. Non-rigid registration of shapes via diffeomorphic point matching. 2004 IEEE international symposium on Biomedical Imaging: *Nano to Macro. (Washington, D.C.),* 2004;1:924–927.
20. Joshi SC, Miller MI. Landmark matching via large deformation diffeomorphisms. *IEEE Trans Image Process*. 2000;9:1357–1370. doi: 10.1109/83.855431.
21. Lehmann E, D' Abrera H. *Nonparametrics: Statistical Methods Based on Ranks*. New York, NY: Springer Science; 2006.
22. Miller MI, Trouve A, Younes L. On the metrics and euler-lagrange equations of computational anatomy. *Annu Rev Biomed Eng*. 2002;4:375–405. doi: 10.1146/annurev.bioeng.4.092101.125733.
23. Lombaert H, Grady L, Pennec X, Ayache N, Cheriet F. Spectral Log-Demons: Diffeomorphic Image Registration with Very Large Deformations. *Int J Comput Vision*. 2014; 107:254–271.
24. Durrleman S, Pennec X, Trouvé A, Braga J, Gerig G, Ayache N. Toward a comprehensive framework for the spatiotemporal statistical analysis of longitudinal shape data. *Int J Comput Vis*. 2013;103:22–59. doi: 10.1007/s11263-012-0592-x.
25. Ardekani S, Weiss RG, Lardo AC, George RT, Lima JA, Wu KC, Miller MI, Winslow RL, Younes L. Computational method for identifying and quantifying shape features of human left ventricular remodeling. *Ann Biomed Eng*. 2009;37:1043–1054. doi: 10.1007/s10439-009-9677-2.
26. Grewal J, Suri R, Mankad S, Tanaka A, Mahoney DW, Schaff HV, Miller FA, Enriquez-Sarano M. Mitral annular dynamics in myxomatous valve disease: new insights with real-time 3-dimensional echocardiography. *Circulation*. 2010;121:1423–1431. doi: 10.1161/CIRCULATIONAHA.109.901181.
27. Mahmood F, Subramaniam B, Gorman JH III, Levine RM, Gorman RC, Maslow A, Panzica PJ, Hagberg RM, Karthik S, Khabbaz KR. Three-dimensional echocardiographic assessment of changes in mitral valve geometry after valve repair. *Ann Thorac Surg*. 2009;88:1838–1844. doi: 10.1016/j.athoracsur.2009.07.007.
28. Ge L, Morrel WG, Ward A, Mishra R, Zhang Z, Guccione JM, Grossi EA, Ratcliffe MB. Measurement of mitral leaflet and annular geometry and stress after repair of posterior leaflet prolapse: virtual repair using a patient-specific finite element simulation. *Ann Thorac Surg*. 2014;97:1496–1503. doi: 10.1016/j.athoracsur.2013.12.036.
29. Ryan LP, Jackson BM, Eperjesi TJ, Plappert TJ, St John-Sutton M, Gorman RC, Gorman JH 3rd. A methodology for assessing human mitral leaflet curvature using real-time 3-dimensional echocardiography. *J Thorac Cardiovasc Surg*. 2008;136:726–734. doi: 10.1016/j.jtcvs.2008.02.073.
30. Xu C, Brinster CJ, Jassar AS, Vergnat M, Eperjesi TJ, Gorman RC, Gorman JH 3rd, Jackson BM. A novel approach to *in vivo* mitral valve stress analysis. *Am J Physiol Heart Circ Physiol*. 2010;299:H1790–H1794. doi: 10.1152/ajpheart.00370.2010.
31. Joudinaud TM, Kegel CL, Flecher EM, Weber PA, Lansac E, Hvass U, Duran CM. The papillary muscles as shock absorbers of the mitral valve

complex. An experimental study. *Eur J Cardiothorac Surg*. 2007;32:96–101. doi: 10.1016/j.ejcts.2007.03.043.
32. Sanfilippo AJ, Harrigan P, Popovic AD, Weyman AE, Levine RA. Papillary muscle traction in mitral valve prolapse: quantitation by two-dimensional echocardiography. *J Am Coll Cardiol*. 1992;19:564–571.
33. Slaughter WS. The Linearised Theory of Elasticity, Boston: Birkhauser; 2002.
34. Gunning GM, Murphy BP. Determination of the tensile mechanical properties of the segmented mitral valve annulus. *J Biomech*. 2014;47:334–340. doi: 10.1016/j.jbiomech.2013.11.035.
35. Bloom N, Cashon G. Annulus fibrosus calcification of the mitral valve. *Am Heart J*. 1945;30:619–622.
36. Wynn TA. Common and unique mechanisms regulate fibrosis in various fibroproliferative diseases. *J Clin Invest*. 2007;117:524–529. doi: 10.1172/JCI31487.
37. Liu AC, Joag VR, Gotlieb AI. The emerging role of valve interstitial cell phenotypes in regulating heart valve pathobiology. *Am J Pathol*. 2007;171:1407–1418. doi: 10.2353/ajpath.2007.070251.
38. Xu S, Grande-Allen KJ. The role of cell biology and leaflet remodeling in the progression of heart valve disease. *Methodist Debakey Cardiovasc J*. 2010;6:2–7.
39. Cushing MC, Liao JT, Anseth KS. Activation of valvular interstitial cells is mediated by transforming growth factor-beta1 interactions with matrix molecules. *Matrix Biol*. 2005;24:428–437. doi: 10.1016/j.matbio.2005.06.007.

CLINICAL PERSPECTIVE

A paucity of data exists on mitral valve (MV) deformation during the cardiac cycle in man. Three-dimensional (3D) echocardiography now allows dynamic volumetric imaging of the MV apparatus, thus enabling computerized modeling of MV function in health and disease. In this investigation, computerized analysis of 3D echocardiography allowed in vivo, patient-specific quantification of MV strain intensities in normals and in patients with organic MV disease with significant mitral regurgitation. Patients with organic mitral valve disease had increased strain intensities when compared with normals, globally as well as in the anterior and posterior leaflets. The posterior leaflet exhibited higher strain values than anterior leaflets in both normals and organic valves. Higher strain concentrations were systematically noted near the commissures and leaflet boundary zones, whereas lower strain values were noted in the center zone. Higher strain values in the posterior leaflet and its border zones may help explain the higher prevalence of localization of MV annular calcifications to the posterior annulus and the higher prevalence of flail posterior leaflet. Quantification of global and regional strain intensity distribution in vivo may have important implications in further understanding MV disease pathophysiology and progression, and in comparative investigations of surgical techniques involved in MV repair that aim at restoring MV geometry and stress and strain reduction for possible improved durability. Our approach could provide new evaluation tools for noninvasive and patient-specific comparisons between pre- and postmitral valve surgery, as well as for quantitative follow-up of disease evolution in patients with MV pathology.

Patient-Specific Quantitation of Mitral Valve Strain by Computer Analysis of Three-Dimensional Echocardiography: A Pilot Study

Sagit Ben Zekry, Jeff Freeman, Aarti Jajoo, Jiwen He, Stephen H. Little, Gerald M. Lawrie, Robert Azencott and William A. Zoghbi

Circ Cardiovasc Imaging. 2016;9:
doi: 10.1161/CIRCIMAGING.115.003254
Circulation: Cardiovascular Imaging is published by the American Heart Association, 7272 Greenville Avenue, Dallas, TX 75231

Print ISSN: 1941-9651. Online ISSN: 1942-0080

Video: Example of mitral valve tracking and strain intensities displays :

Beginning (0s - 11s) -- Multiple views of static model (Anterior and posterior leaflet) of a patient with organic MV at mid-systole.

Middle (11s - 32s) -- Deformation of model between mid-systole and end-systole. The deformation is shown multiple times (forward and reverse) from multiple angles.

End (33s - 47s) -- Strain Intensity (SI) level lines displayed on snapshot static model at mid-systole. These strain intensities are for the mid-systole to end-systole deformation just shown. High SI is in red/orange, while low SI is in deep blue. Notice the high SI at coaptation, commissures, and along the annulus boundary.